Embryonic stem cell-derived extracellular vesicles rejuvenate senescent cells and antagonize aging in mice

Lu Yu [a], Hang Wen [a], Chang Liu [a], Chen Wang [a], Huaxin Yu [a], Kaiyue Zhang [a], Qingsheng Han [a], Yue Liu [a], Zhongchao Han [c], Zongjin Li [a], Na Liu [a,b,*]

[a] School of Medicine, Nankai University, Tianjin, 300071, China
[b] Key Laboratory of Bioactive Materials, Ministry of Education, College of Life Sciences Nankai University, Tianjin, 300071, China
[c] Institute of Stem Cells, Health-Biotech (Tianjin) Stem Cell Research Institute Co., Ltd, Tianjin, 301700, China

ABSTRACT

Aging is a degenerative process that leads to tissue dysfunction and death. Embryonic stem cells (ESCs) have great therapeutic potential for age-related diseases due to their capacity for self-renewal and plasticity. However, the use of ESCs in clinical treatment is limited by immune rejection, tumourigenicity and ethical issues. ESC-derived extracellular vesicles (EVs) may provide therapeutic effects that are comparable to those of ESCs while avoiding unwanted effects. Here, we fully evaluate the role of ESC-EVs in rejuvenation *in vitro* and *in vivo*. Using RNA sequencing (RNA-Seq) and microRNA sequencing (miRNA-Seq) screening, we found that miR-15b-5p and miR-290a-5p were highly enriched in ESC-EVs, and induced rejuvenation by silencing the *Ccn2*-mediated AKT/mTOR pathway. These results demonstrate that miR-15b-5p and miR-290a-5p function as potent activators of rejuvenation mediated by ESC-EVs. The rejuvenating effect of ESC-EVs was further investigated *in vivo* by injection into aged mice. The results showed that ESC-EVs successfully ameliorated the pathological age-related phenotypes and rescued the transcriptome profile of aged mice. Our findings demonstrate that ESC-EVs treatment can rejuvenate senescence both *in vitro* and *in vivo* and suggest the therapeutic potential of ESC-EVs as a novel cell-free alternative to ESCs for age-related diseases.

Credit Author Statement

Na Liu: Conceptualization, Methodology, Supervision, Funding acquisition, Project administration, Writing – reviewing and editing. Lu Yu: Conceptualization, Methodology, Investigation, Methodology, Visualization, Data curation, Formal analysis, Writing – original draft. Hang Wen: Investigation, Visualization. Chang Liu: Investigation, Writing – reviewing and editing. Chen Wang: Investigation. Huaxin Yu: Investigation. Qingsheng Han: Investigation. Kaiyue Zhang: Investigation. Yue Liu: Investigation. Zhongchao Han: Writing – reviewing and editing. Zongjin Li: Writing- reviewing and editing.

1. Introduction

Aging is characterized by the gradual loss of physiological integrity, organs dysfunction, tissue loss of homeostasis and reduced regenerative capacity [1,2]. Aging is associated with the increased of genomic instability, telomere attrition, epigenetic changes, impaired nutrient perception, mitochondrial dysfunction, cellular senescence, stem cell depletion and altered intercellular communication, which further accelerate aging [3–5]. Several 'rejuvenating' interventions have been proposed to delay aging mainly by targeting the above features. These interventions include metabolic manipulation [6,7], partial reprogramming [8–10], heterochronic parabiosis [11,12], senescent cell ablation [13–16] and stem cell-based therapies [17–19].

Embryonic stem cells (ESCs) are pluripotent stem cells that can self-renew indefinitely and differentiate into any tissue cell in the body [20–22], providing them potential for regenerative applications [23–25]. However, due to immune rejection, tumourigenicity and ethical issues, the use of ESCs in clinical treatment is limited [26–28]. Extracellular vesicles (EVs) are nanoscale membrane bubbles secreted by cells that transport various cellular biomolecules into recipient cells, including mRNAs, miRNAs, ncRNAs and proteins [29,30]. ESC-EVs have the therapeutic potential of ESCs and successfully avoid immunogenicity [31] and tumourigenesis [32], which can be used as an ideal cell-free alternative to ESCs in clinical treatment.

The senescence-associated secretory phenotype (SASP), including several soluble factors and EVs secreted by senescent cells, is the main hallmark of aging [33]. Change of SASP by parabiosis [11] and partial reprogramming [8] could rejuvenate aged mice, suggesting that factors

derived from young cells or pluripotent stem cells could prevent senescence. We therefore hypothesized that senescence could be ameliorated by EVs derived from ESCs, which have an unlimited capacity for self-renewal and retain pluripotency. Recent studies from our group and others have shown that ESC-EVs play an important role in rejuvenating senescence, partly by enhancing the functions of adult stem cells *in vivo* [17,34–37]. However, many issues remain unresolved, such as which components in ESC-EVs play a role in rejuvenating aging and the mechanism. Here, we aimed to determine the roles and mechanisms of ESC-EVs in rejuvenation. Our data demonstrate that ESC-EVs can ameliorate senescence both *in vitro* and *in vivo*. Using miRNA-Seq and RNA-Seq, we identify two enriched miRNAs in ESC-EVs, miRNA-15b-5p and miRNA-290a-5p, which prevent senescence by targeting the *Ccn2* and inactivating the AKT/mTOR signaling pathway.

2. Results

2.1. Extracellular vesicles isolated from embryonic stem cells ameliorate senescence in vitro

Extracellular vesicles were isolated by ultracentrifugation from conditioned media of ESCs and MEFs (Mouse embryonic fibroblasts, control), respectively (Fig. S1A). ESC-EVs and MEF-EVs were then characterized in terms of morphology by transmission electron microscopy (TEM), particle size by nanoparticle tracking analysis (NTA) and surface markers by Western blot. Western blot analysis showed the presence of the exosomal protein markers Alix, TSG101 and CD63, and the absence of the Golgi-associated protein GM130 in ESC-EVs and MEF-EVs (Fig. S2A). TEM revealed ESC-EVs and MEF-EVs with the typical size
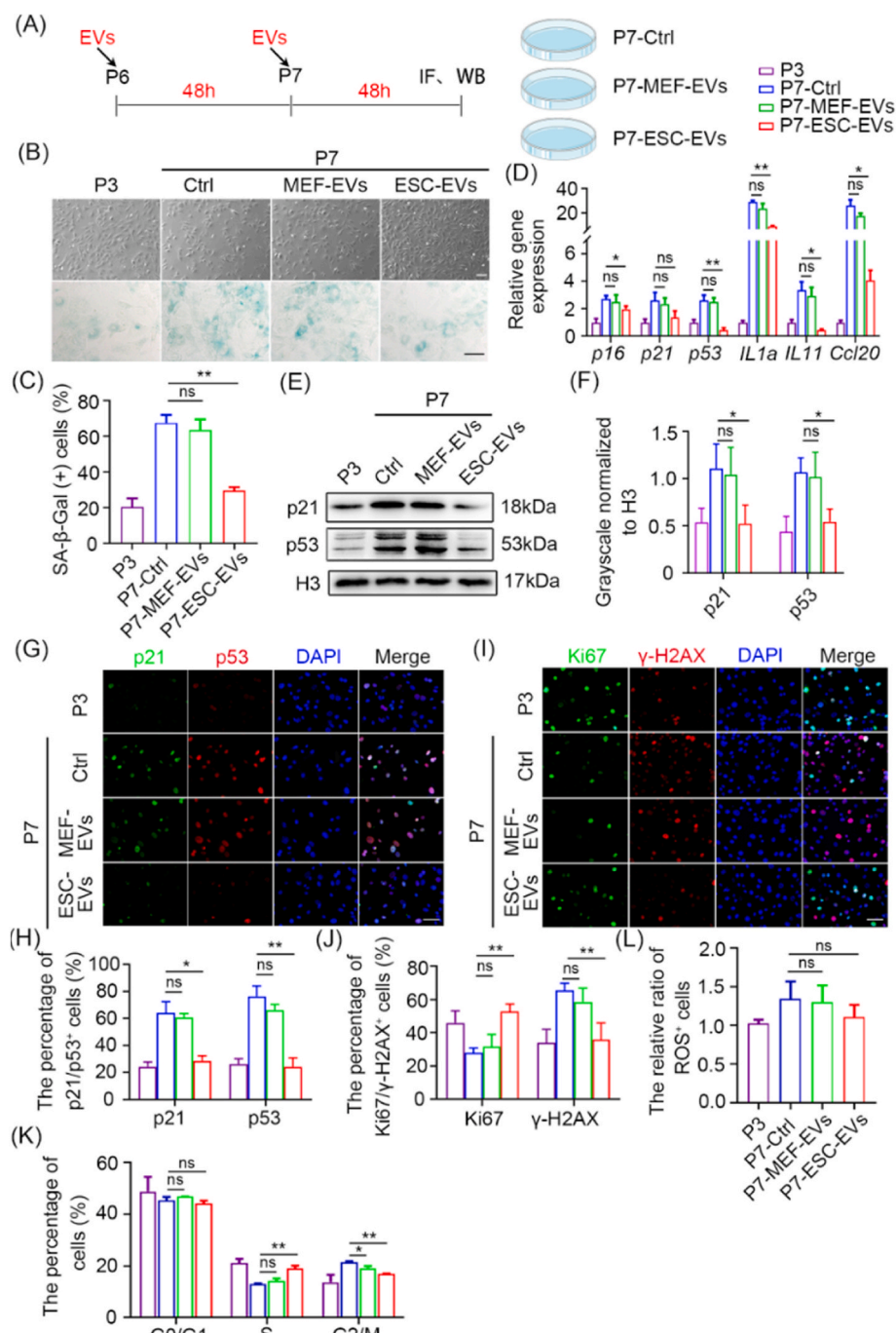
Fig. 1. Antisenescence effects of ESC-EVs on late-passaged MEFs. **(A)** Schematic represention of EVs treating senescent MEFs. After 96 h of treatment with EVs, the 7th generation MEFs were used for subsequent detection. **(B)** Representative cellular morphology and SA-β-gal staining of P3 MEFs, P7 MEFs and P7 MEFs treated with MEF-EVs or ESC-EVs. Scale bar represents 100 μm. **(C)** Quantification of the percentage of SA-β-gal positive MEFs. **(D)** RT-qPCR analysis of senescence-related genes in P3 MEFs and P7 MEFs exposed to MEF-EVs and ESC-EVs, respectively. **(E)** Western blot analysis of p21 and p53 in P3 MEFs and P7 MEFs exposed to MEF-EVs and ESC-EVs, respectively. **(F)** Grayscale statistical analysis of p21 and p53 relative to H3. **(G)** Immunofluorescence analysis of p21 and p53 expression in P3 MEFs and P7 MEFs exposed to MEF-EVs or ESC-EVs. Scale bar represents 100 μm. Bottom panel: Quantification of the percentage of p21 and p53 positive MEFs. **(H)** Immunofluorescence analysis of Ki67 and γ-H2AX expression in P3 MEFs and P7 MEFs exposed to MEF-EVs or ESC-EVs. Scale bar represents 100 μm. Bottom panel: Quantification of the percentage of Ki67- and γ-H2AX-positive MEFs. **(I)** Cell cycle of P3 MEFs and P7 MEFs exposed to MEF-EVs or ESC-EVs were presented by G0/G1, S and G2/M phases. **(J)** Quantification of the ratio of ROS-positive cells in each group to the negative control group. Data are presented as mean ± SEM. n = 3. Student's *t*-test: ns, not significance; *$p < 0.05$ and **$p < 0.01$.

range (80–120 nm in diameter) and characteristic round shape (Fig. S2B). The average particle size of ESC-EVs (~80 nm) was slightly smaller than that of MEF-EVs (~110 nm) (Figs. S2B and C). To verify whether EVs could be internalised into aged MEFs, we labelled EVs with DiI, a fluorescent dye incorporated into membranes, and traced the intracellular localisation of EVs. Immunofluorescence results showed that DiI were colocalized with Tubulin, indicating that EVs were endocytosed into MEFs (Fig. S2D). Time-dependent uptake of DiI-labelled ESC-EVs by MEFs indicated that EVs had been largely internalised by MEFs after 6h (Fig. S1B). Taken together, these data indicate that EVs were successfully isolated from ESCs and could be effectively internalised into ged MEFs.

To evaluate the anti-senescence effect of ESC-EVs, we established the senescent cell model *in vitro* by continuously passaging MEFs for 7 passages (P7 MEFs), which exhibited typical senescence-related characteristics, such as the higher levels of p21 and p53 (Figs. S3A–F) and the increased SA-β-Gal activity (Figs. S3G and H), suggesting that P7 MEFs can be used as a senescence model, and P3 MEF as a young control. We treated the aged MEF with ESC-EVs (100 μg/ml) for 96 h (Fig. 1A; Fig. S4A), and found that the characteristics of senescent MEFs (P7 MEFs), such as flat morphology and a higher level of SA-β-gal activity, were all significantly rescued by ESC-EVs treatment, which was not observed in the MEF-EVs treatment group (Figs. 1B and C). ESC-EVs treatment reversed the expression level of senescence- and SASP-

related genes, including *p16, p21, p53, IL1a, IL11* and *Ccl20*, which were upregulated in senescent cells (P7 MEFs) (Figs. 1D–F). The proportions of p21-and p53-positive MEFs were also reduced by ESC-EVs treatment (Fig. 1G). ESC-EVs treatment rescued the proliferation arrest of senescent MEFs as indicated by increased Ki67-positive cells and decreased γ-H2AX-positive cells (Fig. 1H). Cell cycle analysis confirmed that ESC-EVs treatment ameliorated the cell-cycle arrest by accelerating the G1/S phase transition (Fig. 1I; Fig. S4B). ROS (reactive oxygen species) levels have been shown to be a potentially critical factor for the induction and maintenance of the cell senescence process. Our results showed that ESC-EVs could alleviate the ROS levels of senescent MEFs (Fig. 1J; Fig. S4C). Our data strongly suggest that ESC-EVs ameliorate the senescence-associated phenotype of aged MEFs.

2.2. ESC-EVs rejuvenate the transcriptome profile of aged cells

To investigate the transcriptome profile associated with ESC-EVs-induced rejuvenation in senescent MEFs, we performed RNA-Seq analysis to obtain the transcriptome profiles of P3 MEFs, P7 MEFs, ESC-EVs treated P7 MEFs (Table S1). Bioinformatics analysis revealed that 830 transcripts were upregulated ($p < 0.05$ and $FC \geq 2$) and 601 transcripts were downregulated ($p < 0.05$ and $FC \leq 0.5$) in ESC-EVs treated P7 MEFs compared to P7 MEFs (Fig. 2A; Tables S2 and 3). We found that ESC-EVs treatment significantly inhibited the expression of senescence-
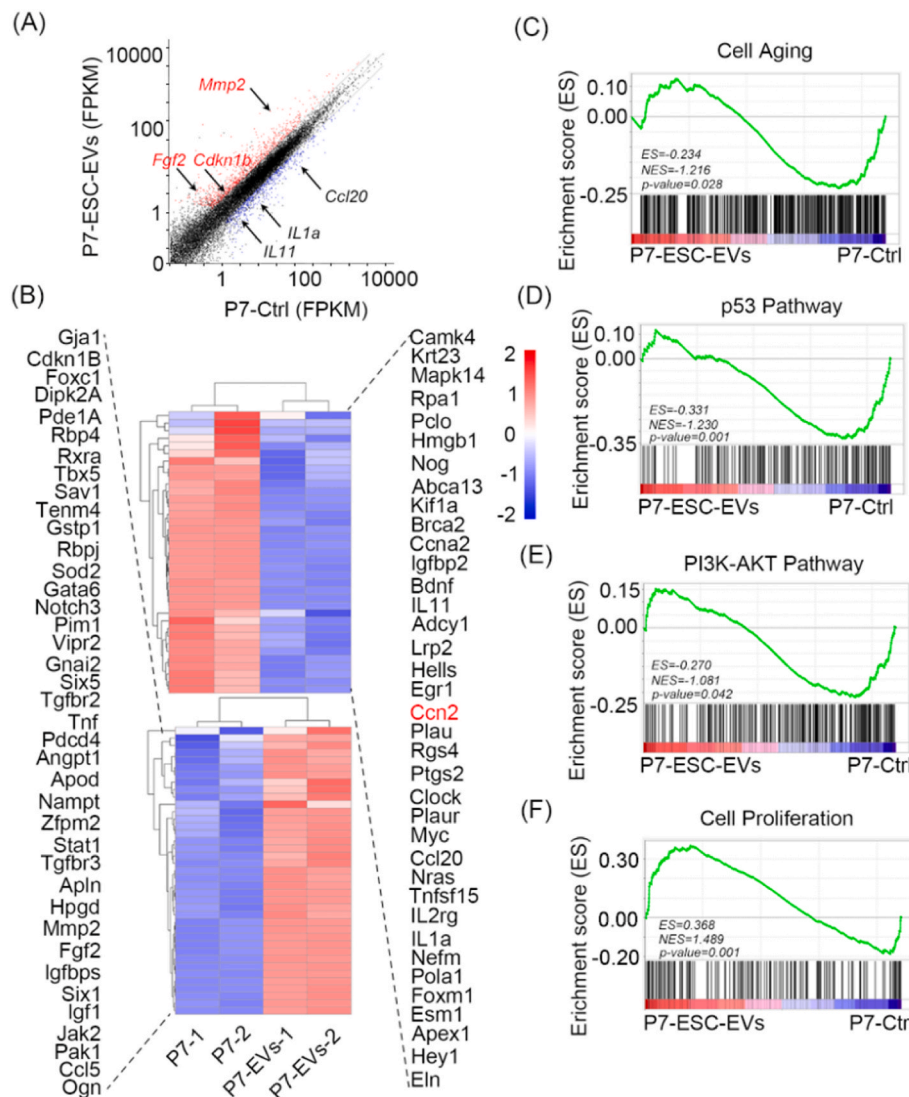
Fig. 2. ESC-EVs rejuvenate the transcriptome profile of senescent MEFs. (A) A scatter plot illustrating differentially regulated gene expression from RNA-Seq analysis between the Ctrl (P7 MEFs) and ESC-EVs treated P7 MEFs. Upregulated and downregulated genes are shown in red and blue, respectively. ($p < 0.05$ and $FC \geq 2$ or $FC \leq 0.5$). **(B)** Heat map of representative cell aging (above) and cell proliferation-related genes (bottom). **(C–F)** GSEA analysis identifies enrichment scores for modules of cell aging (C), p53 pathway (D), PI3K-AKT pathway (E) and cell proliferation (F). ES, enrichment score. NES, normalized enrichment score.

related genes, such as *IL11*, *IL1a*, *Ccl20* and *Ccn2*, while promoting the expression of proliferation-related genes, such as *Cdkn1b* (Fig. 2B). KEGG pathway analysis revealed that ESC-EVs treatment significantly regulated pathways involved in the regulation of aging, including 'Cell cycle', 'MAPK signaling pathway', and 'p53 signaling pathway' (Fig. S5A). GO analysis showed that the differentially expressed genes were involved in the cell cycle and DNA replication (Fig. S5B). Gene set enrichment analysis (GSEA) revealed that ESC-EVs treatment alleviated the enrichment of cell aging, p53 pathway and AKT/mTOR pathway (Figs. 2C–E). In contrast, the enrichment of cell proliferation was enhanced with ESC-EVs treatment (Fig. 2F). Taken together, the RNA-Seq results showed that ESC-EVs treatment significantly rejuvenated the age-related gene expression pattern.

2.3. miRNA landscape of ESC-EVs

Previous studies have reported that EVs can affect the biological behaviors of recipient cells by transferring the encapsulated proteins and miRNAs [38,39]. MiRNAs are endogenous ~22 nt RNAs that can play important regulatory roles by targeting mRNAs for cleavage or translational repression [40]. MiRNAs from EVs effectively alter the transcriptome of recipient cells. MiR-29b-3p in BM-MSC-derived EVs could modulate age-related insulin resistance [41]. Zhang et al. found that central treatment with EVs secreted by healthy hypothalamic stem cells could slow aging, and that the anti-aging effect of hypothalamic stem cells was partially mediated by the miRNAs of EVs secreted from these cells [42]. In light of the above findings and our RNA-Seq results, we focused on miRNAs in ESC-EVs to identify which miRNAs contribute to
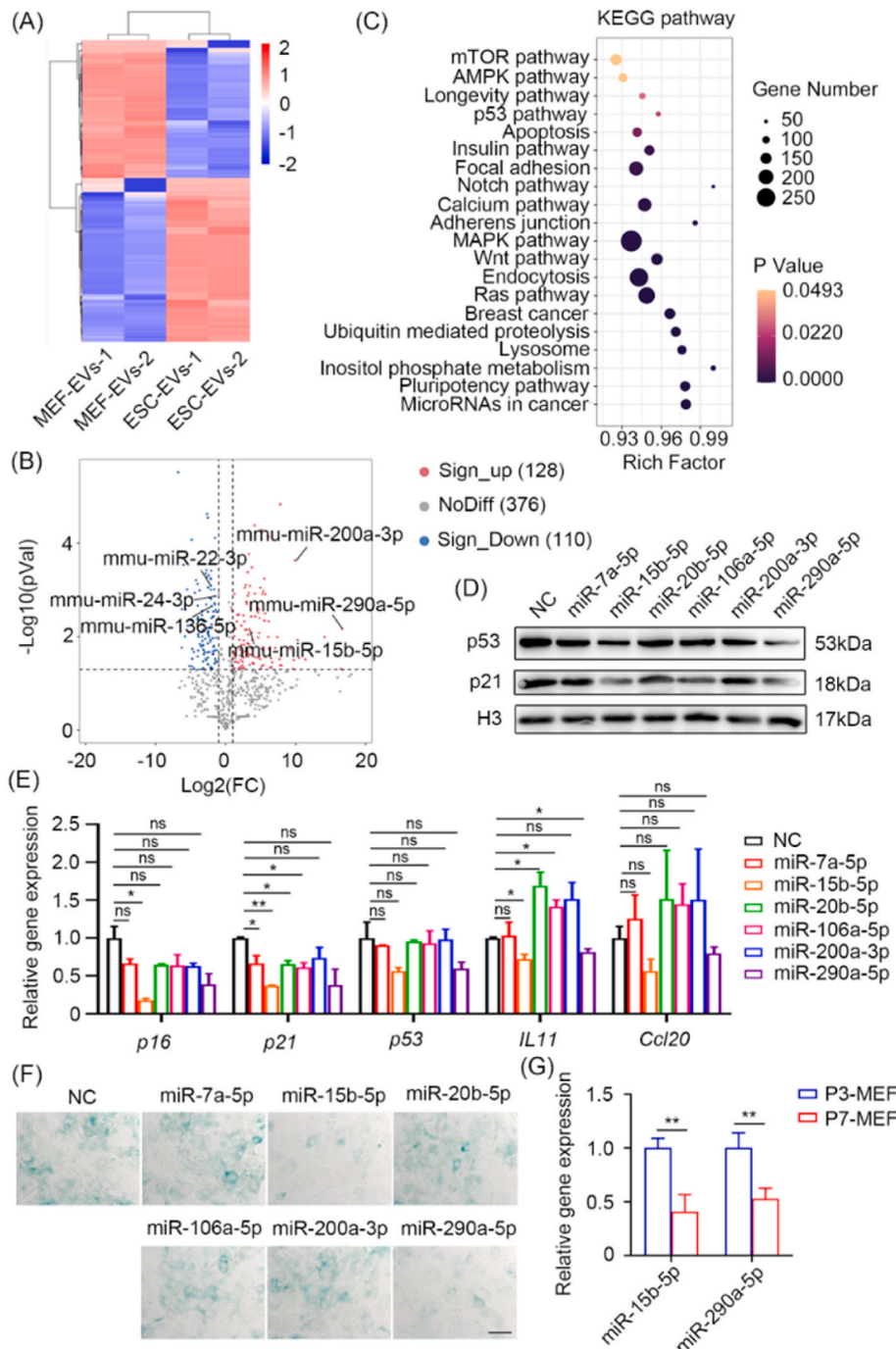

Fig. 3. **miRNA landscape of ESC-EVs.** **(A)** Hierarchical clustering of the miRNA-Seq analysis results shows differentially expressed miRNAs ($p < 0.05$) between the ESC-EVs and MEF-EVs. **(B)** A volcano plot illustrating differential miRNA expression from miRNA-Seq analysis between the ESC-EVs and MEF-EVs. Up-regulated and down-regulated miRNAs are shown in red and blue, respectively. ($p < 0.05$ and FC ≥ 2 or FC ≤ 0.5). **(C)** KEGG pathway analysis of the target genes of significantly enriched miRNAs ($p < 0.05$ and FC ≥ 2) in ESC-EVs vs MEF-EVs. **(D)** Western blot analysis of senescence-related proteins after overexpression of 6 candidate miRNAs in the senescent MEFs. **(E)** RT-qPCR analysis for the expression of senescence-related genes after overexpression of 6 candidate miRNAs in the senescent MEFs. **(F)** SA-β-gal staining of senescent MEFs overexpressing of 6 candidate miRNAs. Scale bar represents 100 μm. **(G)** RT-qPCR analysis for the expression of miR-15b-5p and miR-290a-5p in P3 and P7 MEFs. Data are presented as mean ± SEM. n = 3. Student's *t*-test: ns, not significance; *$p < 0.05$ and **$p < 0.01$.

rejuvenating the age-related gene expression pattern. To determine the miRNAs enriched in ESC-EVs that could be responsible for ameliorating senescence, we performed miRNA sequencing (miRNA-Seq) to identify the miRNAs profile in ESC-EVs. The hierarchical clustering heat map showed the differentially expressed miRNAs between ESC-EVs and MEF-EVs (Fig. 3A). 128 miRNAs were upregulated ($p < 0.05$ and FC $\geq$ 2), and 110 miRNAs were downregulated ($p < 0.05$ and FC $\leq$ 0.5) in ESC-EVs compared to MEF-EVs (Fig. 3B; Tables S4 and 5). Eight differentially expressed miRNAs (6 upregulated: miR-7a-5p, miR-15b-5p, miR-20b-5p, miR-106a-5p, miR-200a-3p, miR-290a-5p and 2 downregulated: miR-22-3p, miR-24-3p in ESC-EVs) were selected and performed RT-qPCR to verify the miRNA-Seq results. RT-qPCR

results were consistent with miRNA-Seq, indicating whihch can be used for further analysis (Fig. S6A). We hypothesized that some specific miRNAs enriched in ESC-EVs have potential rejuvenating effects, so we focused on the 128 upregulated miRNAs, whose target genes were predicted by OmicStudio tools [43,44]. These genes were enriched in age-related signaling pathways such as mTOR pathway, p53 pathway, longevity regulating pathway, focal adhesion, and insulin signaling pathway (Fig. 3C). Furthermore, GO analysis showed that the target genes of upregulated miRNAs were mainly involved in protein transport, protein phosphorylation, etc (Fig. S6B), indicating that miRNAs in ESC-EVs may regulate aging.

We screened the 20 most enriched miRNAs in ESC-EVs and
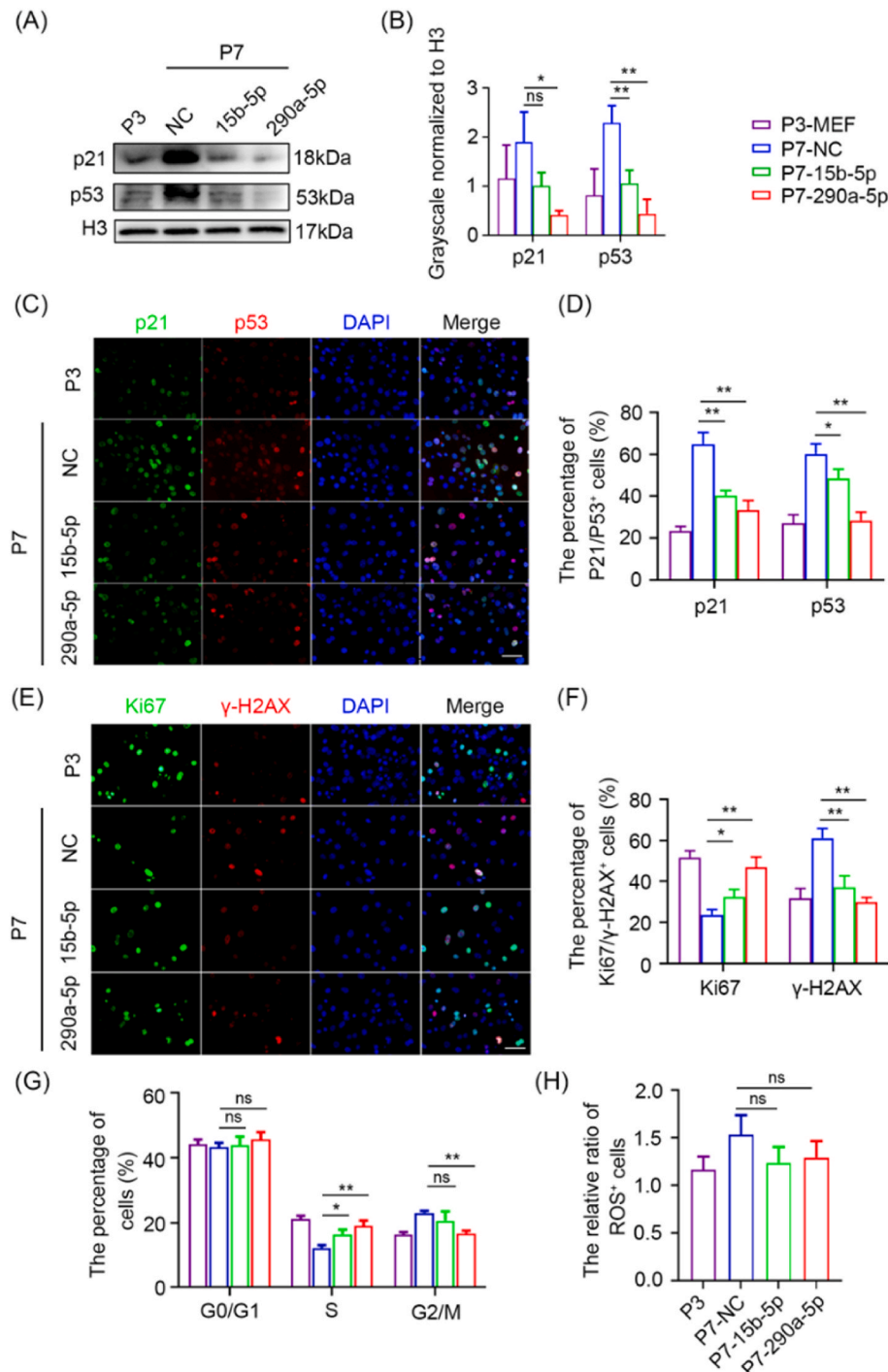
Fig. 4. miR-15b-5p and miR-290a-5p rejuvenate aged cells. (A) Western blot analysis of p21 and p53 in P7 MEFs overexpressing of miR-15b-5p or miR-290a-5p. **(B)** Grayscale statistical analysis of p21 and p53 relative to H3. **(C)** Immunofluorescence analysis of p21 and p53 in P7 MEFs overexpressing of miR-15b-5p or miR-290a-5p. Scale bar represents 100 μm. **(D)** Quantification of the percentage of p21 and p53 positive MEFs respectively. **(E)** Immunofluorescence analysis of Ki67 and γ-H2AX in P7 MEFs overexpressing of miR-15b-5p or miR-290a-5p. Scale bar represents 100 μm. **(F)** Quantification of the percentage of Ki67 and γ-H2AX positive MEFs respectively. **(G)** Cell cycle of P3 MEFs and P7 MEFs overexpressing of miR-15b-5p or miR-290a-5p was depicted by G0/G1, S and G2/M phases. **(H)** Quantification of the ratio of ROS-positive cells in each group to the negative control group. Data are presented as mean $\pm$ SEM. n = 3. Student's *t*-test: ns, not significance; *$p < 0.05$ and **$p < 0.01$.

performed KEGG analysis for their target genes. Relationships between miRNAs and KEGG pathway terms were shown in the chord diagram (Fig. S7). The most prominent miRNAs related to the senescence signaling pathway were miR-7a-5p, miR-15b-5p, miR-20b-5p, miR-106a-5p, miR-200a-3p and miR-290a-5p, which were also down-regulated in aged cells [45] (Fig. S7) and had higher abundance in ESC-EVs (Fig. S8A; Table S6). Therefore, we selected six miRNAs for further verification. Firstly, we overexpressed these six miRNAs by transfecting their mimics into P7 MEFs (Figs. S8B–G), and then the anti-senescence effects were evaluated by determining the expression levels of *p16*, *p53*, *p21* and SA-β-Gal activity. Interestingly, the presence of miR-15b-5p or miR-290a-5p mimics in P7 MEFs induced a significant decrease in the expression levels of *p16*, *p21*, *p53*, *IL11*, *Ccl20* (Figs. 3D and E) and SA-β-Gal activity (Fig. 3F). The expression levels of

miR-15b-5p and miR-290a-5p were higher in young cells (P3 MEF) than that in aged MEFs (P7 MEF) (Fig. 3G), further suggesting that these two miRNAs may be responsible for rejuvenation.

2.4. miR-15b-5p and miR-290a-5p rejuvenate aged cells

Therefore, we next investigated the functions and mechanisms of miR-15b-5p or miR-290a-5p in aging and rejuvenation. Overexpression of miR-15b-5p or miR-290a-5p in senescent MEFs significantly decreased the expression of p21 and p53 (Figs. 4A and B). Figs. 4C and **D** shows that the proportion of p21-and p53-positive cells were reduced in cells overexpressing miR-15b-5p or miR-290a-5p. Similarly, miR-15b-5p or miR-290a-5p promoted the proliferation, as indicated by the significant increase in the percentage of Ki67-positive cells and prevented the
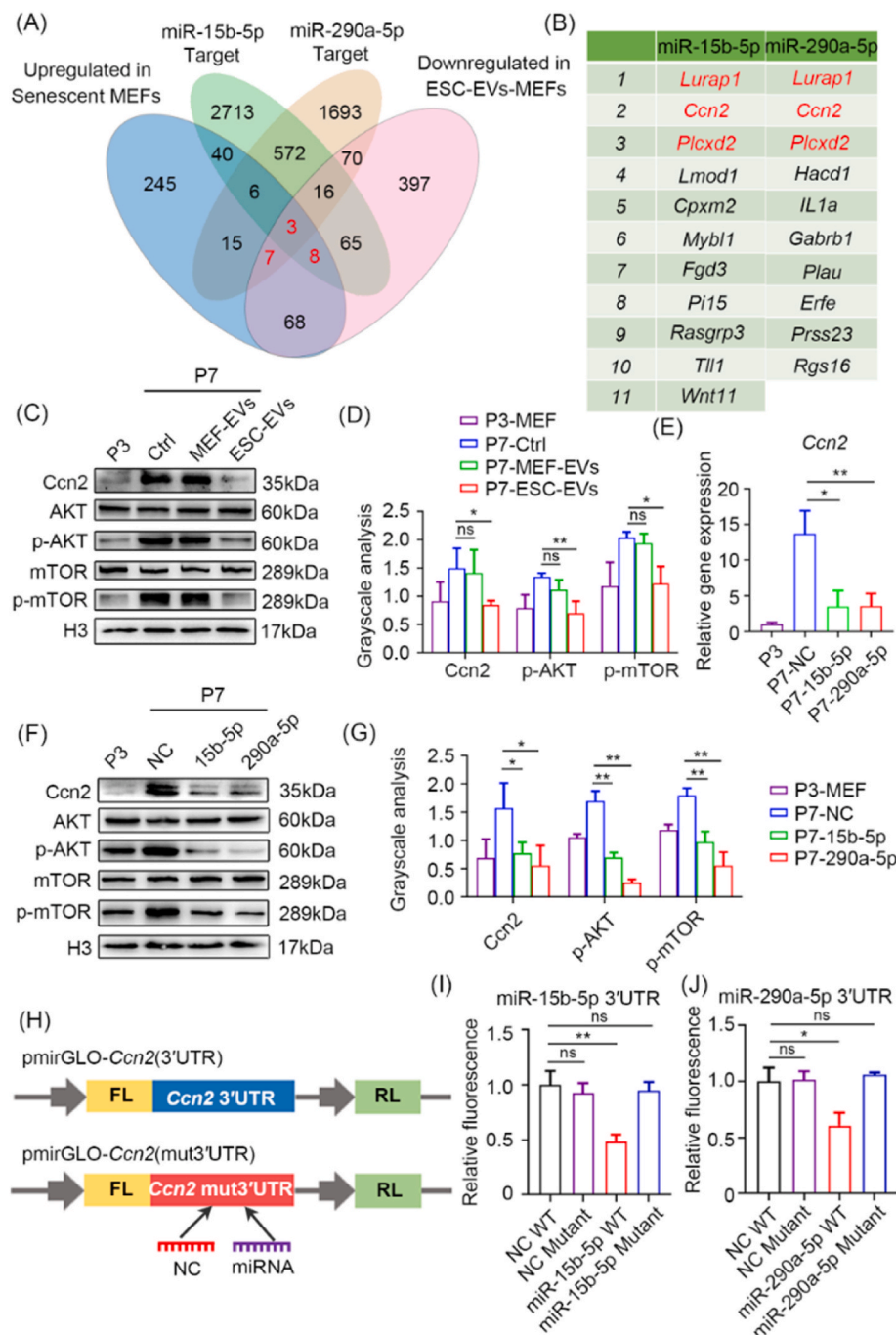

Fig. 5. m**iR-15b-5p and miR-290a-5p target *Ccn2*-mediated AKT-mTOR signaling pathway. (A)** Venn diagram showing overlapping genes up-regulated in senescent MEFs, down-regulated in ESC-EVs-MEFs and target genes of miR-15b-5p or miR-290a-5p. **(B)** The table shows 11 target genes of miR-15b-5p (left) and 10 target genes of miR-290a-5p (right) that are up-regulated in senescent MEFs and down-regulated in ESC-EVs treatment. **(C)** Western blot analysis of Ccn2, AKT, p-AKT, mTOR and p-mTOR levels in P3 MEFs and P7 MEFs exposed to MEF-EVs or ESC-EVs. **(D)** Grayscale statistical analysis of Ccn2 relative to Tubulin, *p*-AKT relative to AKT, *p*-mTOR relative to mTOR. **(E)** RT-qPCR analysis of *Ccn2* transcript levels in P3 MEFs and P7 MEFs overexpressing of miR-15b-5p or miR-290a-5p. **(F)** Western blot analysis of the level of Ccn2, AKT, p-AKT, mTOR and p-mTOR in P3 MEFs and P7 MEFs overexpression of miR-15b-5p or miR-290a-5p. **(G)** Grayscale statistical analysis of Ccn2 relative to Tubulin, *p*-AKT relative to AKT, *p*-mTOR relative to mTOR. **(H)** Luciferase reporter constructs. The dual reporter vector pmirGLO expresses Firefly Luciferase (FL) and Renilla Luciferase (RL) under separate promoters. The plasmid pmir-GLO-*Ccn2* (3′UTR) has the wild-type *Ccn2* 3′UTR of miR-15b-5p or miR-290a-5p binding site inserted directly after the FL coding region; plasmid pmirGLO-*Ccn2* (mut3′UTR) has the *Ccn2* 3′UTR with a mutation in the miR-15b-5p or miR-290a-5p binding site inserted directly following the FL coding region. **(I)** Luciferase activity was measured in 293T cells that were co-transfected with miR-15b-5p mimic or miR-15b-5p NC and luciferase reporter plasmids containing wild-type or mutant. **(J)** Luciferase activity was measured in 293T cells were co-transfected with miR-290a-5p mimic or miR-290a-5p NC and luciferase reporter plasmids containing wild-type or mutant. Data are presented as mean ± SEM. n = 3. Student's *t*-test: ns, not significance; *$p < 0.05$ and **$p < 0.01$.

accumulation of γ-H2AX in aged MEFs (Figs. 4E and F). Rapid phosphorylation of the histone variant H2AX to form γH2AX at Ser-139 is an early cellular response to the DNA double-strand breaks (DSBs). DSBs accelerate the aging process [46]. γ-H2AX is one of the molecular markers of aging. Moreover, miR-15b-5p or miR-290a-5p promoted the G1/S transition (Fig. 4G; Fig. S9A) and alleviated the ROS levels (Fig. 4H; Fig. S9B). Taken together, the results show that miR-15b-5p and miR-290a-5p in ESC-EVs play a role in alleviating senescence.

We speculated that ESC-EVs might transfer miR-15b-5p and miR-290a-5p into the senescent cell and reverse aging by silencing highly expressed target genes in senescent cells. To identify the crucial genes, we performed Venn analysis using the sets of miR-15b-5p target genes, miR-290a-5p target genes, age-related genes, and downregulated genes in ESC-EVs-MEFs (Table S7), and identified 11 target genes of miR-15b-

5p, and 10 target genes of miR-290a-5p (Figs. 5A and B), respectively. There were three common mRNAs in the two lists, *Ccn2*, *Lurap1* and *Plcxd2* (Fig. 5B). Among them, *Ccn2* and *Lurap1* are proteins involved in age-related signaling pathway. Jing et al. have demonstrated that Lurap1 promotes cell aging by activating the NF-κB pathway [47], which was also activated in our aged cells (P7 MEFs) with increased phosphorated-p65 (p-p65) (Figs. S10A and B). However, miR-15b-5p or miR-290a-5p only slightly affected the NF-κB signaling pathway (Figs. S10A and B), while ESC-EVs treatment significantly prevents Ccn2 expression and AKT activation in aged MEFs (Figs. 2E and 5C, D). So, we focused on Ccn2 (Cellular Communication Network Factor 2) as it has been established to be prominence in senescence and AKT pathway activation [48–52]. *Ccn2* had a higher expression level in aged cells (P7 MEFs), which could be downregulated by miR-15b-5p or miR-290a-5p
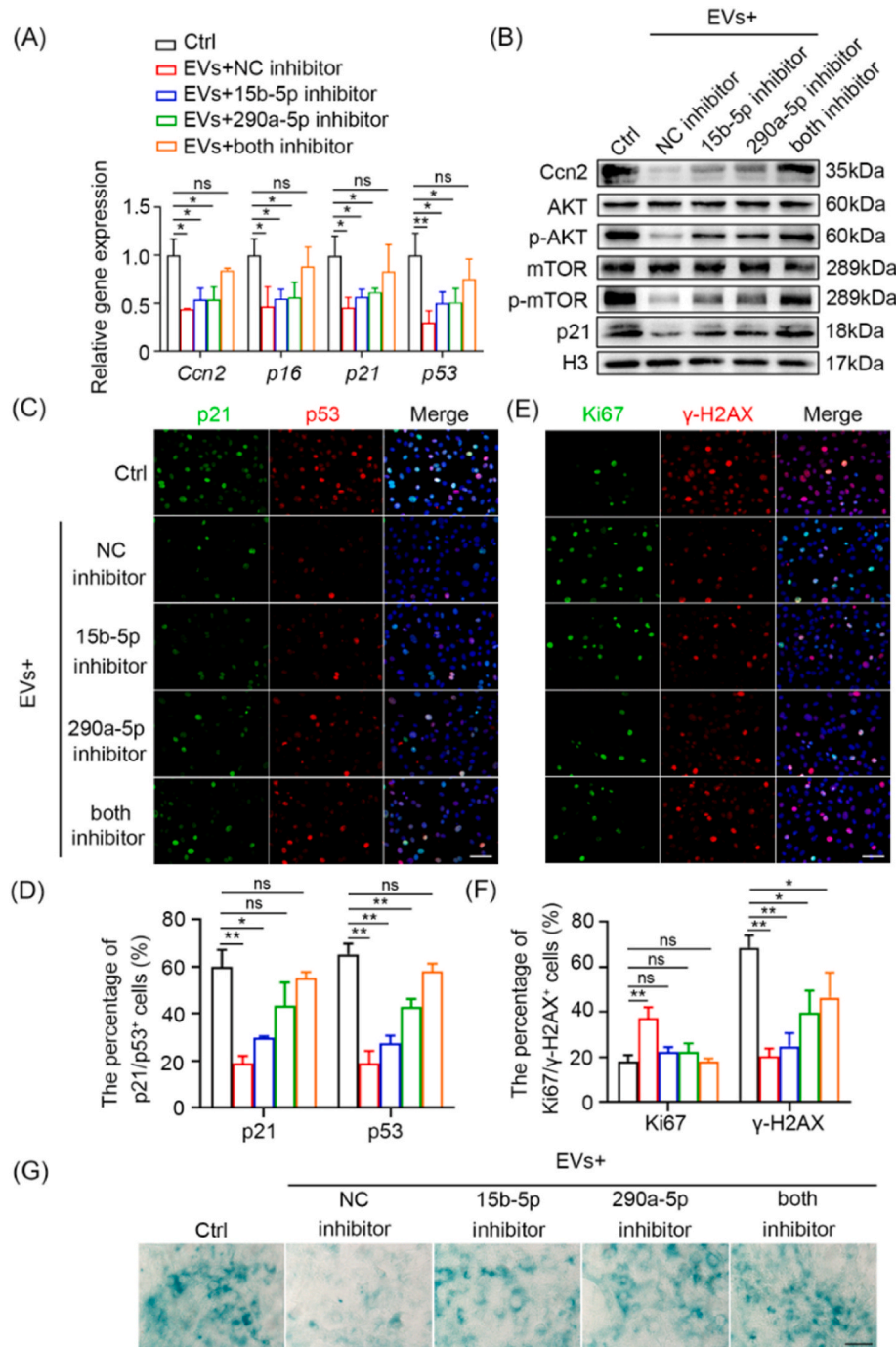

Fig. 6. ESC-EVs alleviate the senescence through miR-15b-5p- and miR-290a-5p. (A) RT-qPCR analysis of senescence-related genes in P7 MEFs, ESC-EVs treated P7 MEFs with the addition of inhibitors of miR-15b-5p or miR-290a-5p or both. **(B)** Western blot analysis of the level of Ccn2, AKT, p-AKT, mTOR, p-mTOR and p21 in P7 MEFs, ESC-EVs treated P7 MEFs with the addition of inhibitors of miR-15b-5p or miR-290a-5p or both. **(C)** Immunofluorescence analysis of p21and p53 in P7 MEFs, ESC-EVs treated P7 MEFs with the addition of inhibitors of miR-15b-5p or miR-290a-5p or both. Scale bar represents 100 μm. **(D)** Quantification of the percentage of p21 and p53 positive MEFs respectively. **(E)** Immunofluorescence analysis of Ki67 and γ-H2AX in P7 MEFs, ESC-EVs treated P7 MEFs with the addition of inhibitors of miR-15b-5p or miR-290a-5p or both. Scale bar represents 100 μm. **(F)** Quantification of the percentage of Ki67 and γ-H2AX positive MEFs respectively. **(G)** SA-β-gal staining of P7 MEFs, ESC-EVs treated P7 MEFs with the addition of inhibitors of miR-15b-5p or miR-290a-5p or both. Scale bar represents 100 μm. Data are presented as mean ± SEM. n = 3. Student's *t*-test: ns, not significance; *$p < 0.05$ and **$p < 0.01$.

(Figs. 5E–G). Phosphorylated AKT and mTOR were increased in P7 MEFs, which were efficiently inhibited by miR-15b-5p or miR-290a-5p (Figs. 5F and G). To verify the direct regulation of the miR-15b-5p and miR-290a-5p on *Ccn2*, we first used RNA-hybrid to identify the potential binding sites of miR-15b-5p and miR-290a-5p. Systematic bioinformatic analysis revealed that miR-15b-5p and miR-290a-5p could bind to the 3′UTR of *Ccn2* (the binding site is shown in Figs. S10C and D). We performed a dual-luciferase assay to verify that miR-15b-5p or miR-290a-5p regulates *Ccn2* expression through direct binding to the 3′UTR. miR-15b-5p or miR-290a-5p significantly decreased the luciferase activity of the *Ccn2* 3′UTR reporter, but had no effect on the reporter with mutation of the binding site, further indicating that *Ccn2* is the direct target of miR-15b-5p or miR-290a-5p (Figs. 5H–J).

2.5. ESC-EVs alleviate the senescence by miR-15b-5p and miR-290a-5p regulating Ccn2

From the above results, we know that miR-15b-5p and miR-290a-5p possess the ability of anti-senescence, so next, we further investigated their roles in the ability of ESC-EVs to rejuvenate by using their specific inhibitors. We found that inhibition of either miR-15b-5p or miR-290a-5p slightly attenuated the anti-senescence effects of ESC-EVs. However, after inhibition of both miR-15b-5p and miR-290a-5p, the rejuvenation phenotype of ESC-EVs almost disappeared (Figs. 6A and B). A combination of miR-15b-5p and miR-290a-5p inhibitors treatment completely neutralized the anti-senescence effect of ESC-EVs on the aged MEF, as evidenced by the increased expression levels of p53, p21, Ki67 and γ-H2AX (Figs. 6C–F). Treatment of the aged MEF with ESC-EVs together with miR-15b-5p and miR-290a-5p inhibitors failed to reduce SA-β-Gal-positive cells (Fig. 6G). Furthermore, miR-15b-5p or miR-290a-5p inhibitors reactivated the AKT signaling pathway which was inhibited by
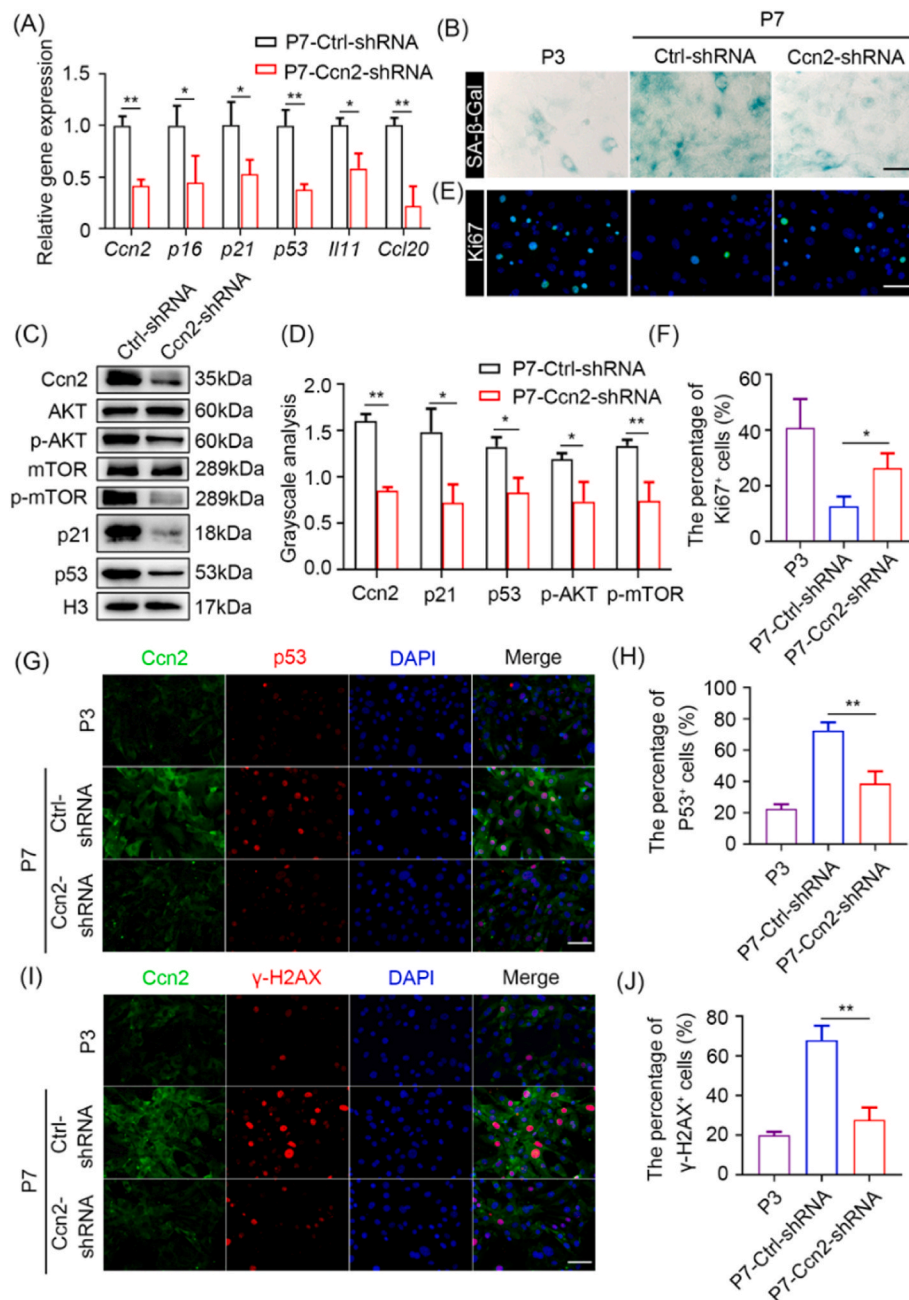
Fig. 7. ***Ccn2* plays an important role in cell senescence. (A)** RT-qPCR analysis of senescence-related genes in ctrl P7 MEFs and Ccn2 knockdown P7 MEFs. **(B)** SA-β-gal staining of P3 MEFs, ctrl P7 MEFs and Ccn2 knockdown P7 MEFs. Scale bar represents 100 μm. **(C)** Western blot analysis of the levels of Ccn2, AKT, *p*-AKT, mTOR, *p*-mTOR, p21 and p53 in ctrl P7 MEFs and Ccn2 knockdown P7 MEFs. **(D)** Grayscale statistical analysis of Ccn2, p21 and p53 relative to H3, *p*-AKT relative to AKT, *p*-mTOR relative to mTOR. **(E)** Immunofluorescence analysis of Ki67 in P3 MEFs, ctrl P7 MEFs and Ccn2 knockdown P7 MEFs. Scale bar represents 100 μm. **(F)** Quantification of the percentage of Ki67 positive MEFs. **(G)** Immunofluorescence analysis of Ccn2 and p53 in P3 MEFs, ctrl P7 MEFs and Ccn2 knockdown P7 MEFs. Scale bar represents 100 μm. **(H)** Quantification of the percentage of p53 positive MEFs. **(I)** Immunofluorescence analysis of Ccn2 and γ-H2AX in P3 MEFs, ctrl P7 MEFs and Ccn2 knockdown P7 MEFs. Scale bar represents 100 μm. **(J)** Quantification of the percentage of γ-H2AX positive MEFs. Data are presented as mean ± SEM. n = 3. Student's *t*-test: ns, not significance; *$p < 0.05$ and **$p < 0.01$.

ESC-EVs in senescent MEFs (Fig. 6B), suggesting that miR-15b-5p and miR-290a-5p are crucial for the rejuvenating effect of ESC-EVs. Our results indicate that ESC-EVs alleviate the senescence of MEFs through miR-15b-5p and miR-290a-5p.

In addition to the preventing the anti-senescence effect, miR-15b-5p or miR-290a-5p inhibitors also reversed the reduction of Ccn2 induced by ESC-EVs treatment (Figs. 6A and B). To investigate the anti-senescence role of *Ccn2*, we downregulated *Ccn2* in aged MEFs using RNA interference. *Ccn2* knockdown significantly decreased the expression of age-related genes (Figs. 7A and C), and SA-β-Gal activity (Fig. 7B). *Ccn2* knockdown significantly inactivated the AKT/mTOR signaling pathway (Figs. 7C and D). *Ccn2* knockdown in senescent MEFs reversed the aged phenotype, as indicated by the decrease in the proportion of p53-positive and γ-H2AX-positive cells (Figs. 7G–J).

Meanwhile, the proliferative capacity was restored (Figs. 7E and F), suggesting that *Ccn2* plays an important role in senescence. Together, these results indicate that miR-15b-5p and miR-290a-5p play crucial roles in the anti-senescence effect of ESC-EVs by silencing the Ccn2-PI3K signaling pathway.

2.6. Rejuvenation of aged mice by ESC-EVs

Next, the anti-senescence effects of ESC-EVs were further evaluated *in vivo* using 14-month-old C57BL/6 mice. As shown in Fig. 8A, we injected 100 µg ESC-EVs by intraperitoneal injection every two days for 8 weeks, and the equivalent volume of PBS injection served as the sham (Fig. 8A). We isolated mouse peripheral blood monocytes (PBMCs) and performed RNA-Seq analysis to obtain the transcriptomic profiles of
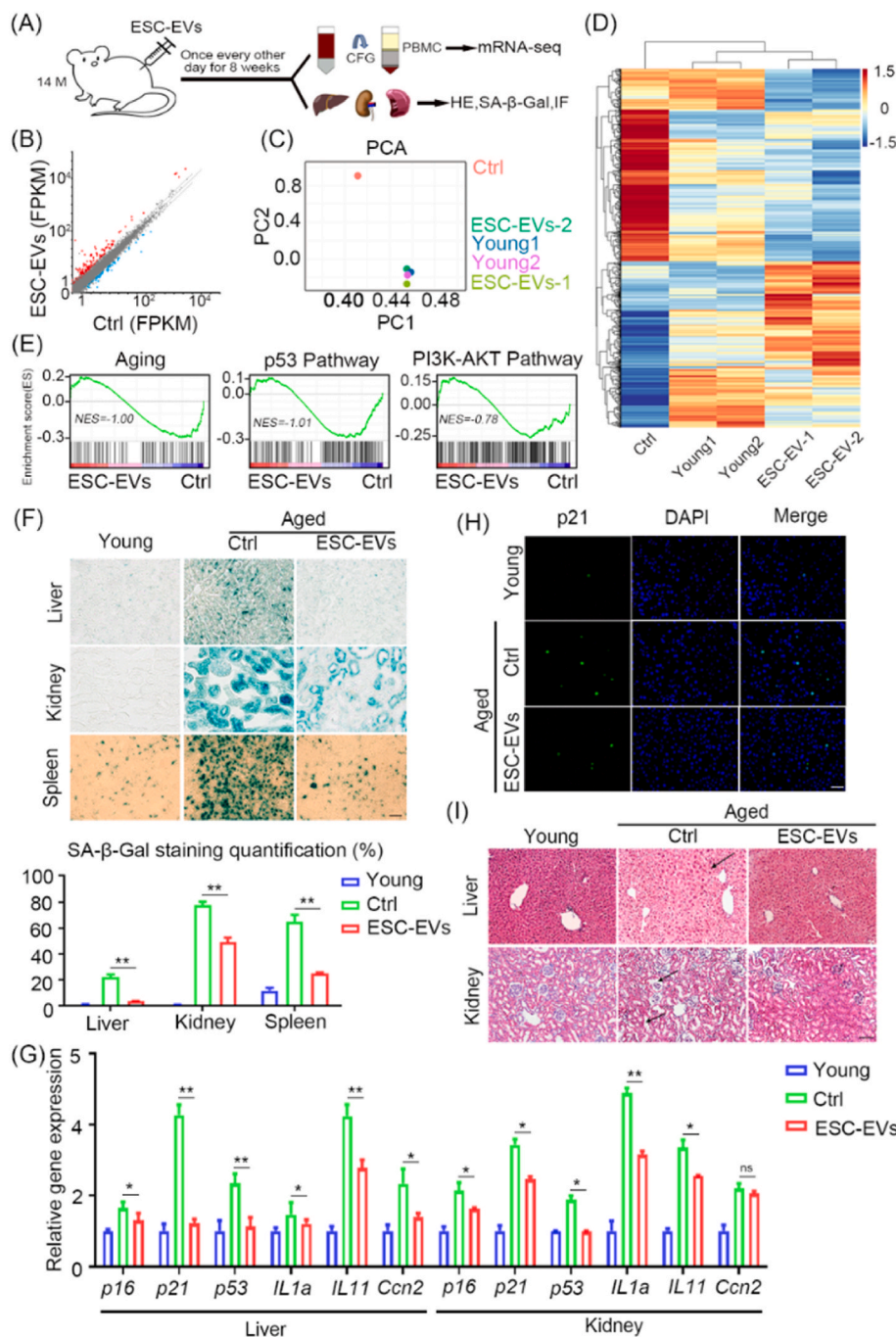
Fig. 8. Rejuvenation of aged mice by ESC-EVs. (A) Schematic illustrating the procedures of the *in vivo* experiment. **(B)** A scatter plot illustrating differentially regulated gene expression from RNA-Seq analysis between the control and ESC-EVs-treated aged mice. Up-regulated and down-regulated genes are shown in red and blue, respectively. ($p < 0.05$ and FC ≥ 2 or FC ≤ 0.5). **(C)** PCA of RNA-Seq of PBMCs from young mice, aged mice, and ESC-EVs-treated aged mice. **(D)** Heat map of differentially regulated genes ($p < 0.05$ and FC ≥ 1.5 or FC ≤ 0.67) expression from RNA-Seq analysis between the aged mice and ESC-EVs treated aged mice. **(E)** GSEA analysis identifies enrichment scores for modules of aging, p53 pathway and PI3K-AKT pathway. **(F)** Representative tissue morphology and SA-β -Gal staining of liver, kidney and spleen after ESC-EVs treatment, and quantification of the percentage of SA-β -Gal positive area. Scale bar represents 100 µm. **(G)** RT-qPCR analysis of senescence-related genes in liver and kidney after ESC-EVs treatment. **(H)** Immunofluorescence analysis of p21 expression in the liver after ESC-EVs treatment. Scale bar represents 100 µm. **(I)** HE staining was used for histological analysis of the liver and kidney after 8 weeks of ESC-EVs treatment. In HE staining of the liver, the arrows indicate the pathological features of hepatocyte enlargement and hepatic cord disruption. In the HE staining of the kidney, the arrows at the top indicate the enlargement of the renal cystic cavity and the glomerular pyknosis, while the arrows at the bottom indicate thinning of the renal tubular wall and enlargement of the lumen. Scale bar represents 100 µm. Data are presented as mean ± SEM. n = 3. Student's *t*-test: ns, not significance; *$p < 0.05$ and **$p < 0.01$.

young mice, aged mice, and those treated with ESC-EVs. The scatter plot showed that 360 transcripts were upregulated ($p < 0.05$ and FC $\geq$ 2) and 142 transcripts were downregulated ($p < 0.05$ and FC $\leq$ 0.5) in ESC-EVs-treated aged mice compared with the control group (Fig. 8B). The RNA-Seq datasets were subjected to Principal Component Analysis (PCA), which showed that the Young and ESC-EVs groups were clustered in space, suggesting that ESC-EVs-treated old mice had a similar transcriptome pattern of mRNAs to that of young mice (Fig. 8C). The clustering heat map of gene expression showed consistent results with PCA (Fig. 8D). GSEA revealed that the signature genes for 'aging', 'p53 pathway' and 'PI3K-AKT pathway' were attenuated by ESC-EVs-treatment (Fig. 8E). The GO analysis of biological processes revealed an enrichment of proteins involved in the regulation of 'aging', 'MAPK signaling' and 'NF-κB signaling' (Fig. S11A). KEGG pathway analysis revealed that ESC-EVs exposure was involved in the regulation of age-related diseases, including 'Parkinson's disease', 'Alzheimer's disease' and 'Huntington's disease' (Fig. S11B). Taken together, these data show that ESC-EVs significantly drive broad transcriptional changes associated with anti-senescence.

In addition, we evaluated the senescence of several organs (such as the spleen, kidney and liver) by detecting the levels of SA-β-Gal, p21, p53 and Ki67. We observed that treatment of old mice with ESC-EVs reduced the level of SA-β-Gal in the sections of the liver, kidney and spleen (Fig. 8F) and decreased the expression of age-related genes, such as *p16*, *p21*, *p53*, *IL1a* and *IL11* in aged mice (Fig. 8G). ESC-EVs treatment significantly inhibited *Ccn2* expression in the liver of aged mice, but showed no significant inhibition in the kidney (Fig. 8G). Immunofluorescence results also showed that ESC-EVs treatment decreased the proportion of p21-and p53-positive senescent cells and increased the propotion of Ki67-positive proliferating cells in aged mice (Fig. 8H; Figs. S12A–E). The heat map of age-related genes also indicated that ESC-EVs treatment could alter gene expression patterns in PBMCs of aged mice (Fig. S12F). HE staining showed that ESC-EVs treatment ameliorated the pathological phenomena of hepatic lobule structure, hepatic cord disorder, hepatocyte enlargement, renal cystic cavity enlargement, glomerular pyknosis, renal tubular wall thinning, lumen enlargement and other pathological phenomena in aged mice (Fig. 8I). Collectively, these data demonstrated that ESC-EVs efficiently ameliorate aging *in vivo*.

3. Discussion

Aging is the biggest risk factor for many diseases. A few decades ago, rejuvenation or amelioration of aging seemed impossible. However, in the last decades, the concept of parabiosis and partial reprogramming with pluripotency-related factors has changed our view on the subject, indicating that factors derived from young cells prevent senescence [8,9, 53]. Sahu et al. found that young circulating extracellular vesicles can regenerate aged muscle [54,55]. Previously, we found that EVs derived from ESCs could rejuvenate the aged MSCs (mesenchymal stem cells) and rescue their regenerative capacity [17]. Recently, several rejuvenation factors enriched in ESC-EVs or ESC-CM (conditioned medium) have been identified, such as TGF-β, Smad2, PDGF-BB (platelet-derived growth factor-BB), miR-291a-3p, miR-294 and miR-200a [34,35,37,56]. However, the roles and mechanisms of ESC-EVs *in vivo* are unknown. Here, we investigate the antisenescence effects of ESC-EVs *in vivo* using aged mice. Our data show that ESC-EVs treatment rescues the transcriptome profile of aged mice and ameliorates the senescence status of several aged organs, providing evidence that ESC-EVs may be candidates for the therapy of various age-related diseases. Jorge et al. found that EVs from young adipose-derived stem cells improved motor coordination, grip strength, fatigue resistance and significantly reduced frailty in aged mice [57]. However, the effects of ESC-EVs treatment on cognitive function and motor activity in aged mice remain unclear and require further investigation.

Furthermore, we identify miR-15b-5p and miR-290a-5p, which are

enriched in ESC-EVs and exert rejuvenating effects by silencing of the *Ccn2*-mediated AKT signaling pathway. MiRNAs, the prominent factors in EVs, have been identified to regulate cellular senescence. For example, miR-504, miR-125b, miR-25 and miR-30d directly bind p53, reduce p53 expression, and rescue p53-mediated cell cycle arrest [58, 59]. To identify the effective antisenescence factors in ESC-EVs, we performed miRNA-Seq and found that miR-15b-5p and miR-290a-5p are crucial for ESC-EVs rejuvenation. Their target gene of *Ccn2* is upregulated in aged cells and can be rescued by ESC-EVs treatment. Ccn family members regulate cell adhesion, migration, proliferation, differentiation, apoptosis, survival and senescence [60]. Ccn1 and Ccn2 (CTGF) are two highly homologous members of the Ccn family that share common structural features, including the conservation of four structural domains with sequence homologies to insulin-like growth factor binding proteins (IGFBPs) and binding sites for several integrin receptors [61, 62]. Several studies have shown that Ccn2 induces cellular senescence [48–50] and activates the PI3K/AKT signaling pathway [51,52], suggesting that *Ccn2* may be a potential target for anti-aging. Using a dual luciferase assay, we found that miR-15b-5p and miR-290a-5p silenced *Ccn2*, thereby inhibiting the Ccn2-dependent AKT signaling pathway and ameliorating the senescence. Here, we demonstrate a novel mechanism for ESC-EVs to protect cells from senescence. However, whether ESC-EVs rejuvenate aged mice via miR-15b-5p and miR-290a-5p remains unknown. Next, we plan to use miR-15b-5p and miR-290a-5p antagonists while treating aged mice with ESC-EVs to further investigate the mechanism by which ESC-EVs resist aging *in vivo*.

In conclusion, our study reveals for the first time a mechanism of rejuvenation of ESC-EVs by transferring miR-15b-5p and miR-290a-5p to senescent cells and then silencing the AKT/mTOR signaling pathway. In addition, we evaluate the anti-senescence effects of ESC-EVs *in vivo*, suggesting a new non-cellular therapeutic tool for aging and age-related diseases. We speculate that the age-related damage would continue to accumulate over time if ESC-EVs therapy were stopped. However, we must be cautious in drawing such conclusions, as longer-term experiments are needed to determine the time period over which ESC-EVs have rejuvenating functions.

4. Materials and methods

4.1. Cell culture

Mouse ESC line D3 (ATCC, CRL-1934) were cultured in DMEM medium (Hyclone) supplemented with 15% FBS (Hyclone), 1% L-glutamine (Corning), 1% NEAA (Gibco), 1% penicillin and streptomycin (Gibco), 1% beta-mercapethanol (Sigma) and 1000 units/mL LIF (Millipore).

Mouse embryonic fibroblasts cells (MEF) were isolated from D13.5 embryos of C57BL/6 mice[3] and were cultured in DMEM medium (Hyclone) containing 10% fetal bovine serum (Hyclone), 1% L-glutamine (Corning) and 1% penicillin and streptomycin (Gibco).

The MEFs were continuously cultured for 7 passages to establish the senescent cell model. The senescent MEFs have a higher level of SA-β-gal and lower proliferative ability *in vitro*.

4.2. Cell proliferation assay

Cell Count Kit 8 (CCK-8) was used to determine the proliferation of MEFs. Briefly, cells were seeded in 96-well plates (2×10^3/well) and treated with different working concentrations of EVs for 48 h or 96 h. Then, 10 μL CCK-8 (TargetMol) solution was added to each well and incubated at 37 °C for 2 h. Optical density (OD) values at 450 nm were read using a microplate analyzer (Promega).

4.3. Extracellular vesicles isolation

Extracellular vesicles were purified from supernatants of ESCs and MEFs as previously described [63,64]. When the cell fusion rate reached

70–80%, the cells were passaged and cultured in DMEM medium with EVs-free serum. After 24 h, the cell culture supernatant was collected and centrifuged at 500 g, 4 °C for 10 min to remove any cells. Centrifuged at 2000 g for 30 min to remove dead cells. Centrifuged at 10,000 g for 30 min to remove cell debris and apoptotic bodies. The supernatant was collected and ultra-centrifuged at 100,000 g for 120 min at 4 °C. The precipitation obtained was the EVs used in this study.

4.4. Extracellular vesicles characterization

The morphology of EVs was observed by transmission electron microscopy (TEM) (Talos F200C, Thermo Fisher). Samples were deposited on a copper grid covered with carbon film (Zhongjingkeyi Technology) and dried at room temperature for 2 min. After removing the excess liquid with a filter, the samples were negatively stained with 2% uranium acetate for 30 s. The samples were air-dried for 60 min and then imaged by TEM. The size of EVs was determined by nanoparticle tracking analysis (NTA) (Particle Metrix).

To verify whether MEFs could internalize EVs, we labelled EVs with CM-DiI membrane dye (Invitrogen) according to the manufacturer's protocol. EVs were mixed with 1 μmol/L CM-DiI and incubated for 5 min at room temperature. Excess dye was removed by ultracentrifugation at 100,000 g for 70 min at 4 °C. The final labelled EVs were resuspended in PBS. CM-DiI labelled EVs were incubated with MEFs for 6 h at 37 °C. After washing the cells with PBS, the cells were fixed with 4% paraformaldehyde. EVs uptake was observed by fluorescence microscopy.

4.5. Generation of Ccn2 knock down (Ccn2-KD) MEFs by RNA interference

Control (GCGTTCAATTAGCAGACCA) and shRNA (GCACCAGTGT-GAAGACATACA) sequences against *Ccn2* mRNA were cloned into pSIREN-RetroQ vector (Clontech). The reconstructed pSIREN-RetroQ vectors were then transfected into senescent MEFs using Lipofectamine 2000 (Invitrogen). The cells were cultured in non-penicillin or streptomycin culture medium for 24 h, and then selected with puromycin (2 μg/ml) for 24 h. The cells were harvested for subsequent experiments.

4.6. miRNA overexpression or inhibition

The miRNA mimic (50 nM) or inhibitor (100 nM) was transfected into MEFs (5×10^5 cells per well) using Lipofectamine 2000 (Invitrogen). Cells were cultured with non-penicillin or streptomycin culture medium for 48 h and the second transfection was performed at 24 h as described above.

4.7. Western blot analysis

Cells were lysed in RIPA buffer (Solarbio) in the presence of a 1 mM protease inhibitor (Solarbio) at 4 °C for 30 min. The sample was then centrifuged at 4 °C, 13,000 rpm for 15 min and the supernatant was collected. The protein concentration was determined according to the manufacturer's instructions using a BCA Protein Analysis Kit (Genstar). Finally, the samples were boiled at 95 °C for 10 min. The obtained protein samples were separated by 10% SDS-PAGE and then transferred to polyvinylidene difluoride (PVDF) membrane (Millipore). After blocking with 5% nonfat milk for 2 h, the PVDF membrane was incubated with primary antibody at 4 °C overnight and then with HRP-conjugated secondary antibody at room temperature (RT) for 2 h. The following antibodies were used at the indicated dilutions: Alix (Abcam, ab275377), TSG101 (Huaan, ET1701-59), CD63 (Abcam, ab217345), GM130 (Abcam, ab52649), p21 (Abcam, ab188224), p53 (CST, 2524), P65 (CST, 8242-T), p-P65 (CST, 3033T), AKT (CST, 4691T), *p*-AKT (CST, 4060T), mTOR (CST, 2983T), *p*-mTOR (CST, 5536T), Ccn2 (ABclonal), H3 (Abcam, ab1791), Tubulin (Proteintech, 66031).

4.8. Quantitative real-time PCR

Total RNA was extracted from the cells or tissues using TRIzol (Invitrogen) according to manufacturer's instructions. 1 μg of RNA was reverse transcribed into cDNA using the first-strand cDNA synthesis system (Roche). Real-time PCR was performed on the Opticon® system (Bio-Rad) using Hieff™ qPCR SYBR® Green Master Mix (No Rox) (Yeasen) in 20 μl reaction volumes. The $2^{-\Delta\Delta Ct}$ method was used to analyze the relative gene expression. The primer sequences used in this study are listed in .Supplementary Tables 8 and 9

4.9. Immunofluorescence

Cells were fixed with 4% formaldehyde in PBS for 10 min at RT. After fixation, cells were treated with 0.1% Triton X-100 in PBS for 30 min at RT. After blocking with 10% normal goat serum for 2 h, cells were incubated with the primary antibody at 4 °C overnight, followed by washing in PBS three times and incubation with the corresponding secondary antibody for 2 h at RT. The following antibodies were used at the indicated dilutions: Ki67 (Abcam, ab16667), γ-H2AX (CST, 80312), p21 (Abcam, ab188224), p53 (CST, 2524).

4.10. Senescence-associated β-galactosidase (SA-β-gal) staining

Cells were washed with PBS and fixed in staining fixative for 15 min at RT. Fixed cells were stained with fresh SA-β-gal staining solution at 37 °C overnight (Beyotime Biotechnology). On the second day, cells stained overnight were washed three times with PBS and imaged under a microscope.

4.11. Reactive oxygen species (ROS) detection assay

DCFH-DA was diluted 1:1000 with the serum-free medium to give a final concentration of 10 μmol/L. The cell culture medium was removed, and 1 ml of diluted DCFH-DA was added to the cells in one well of the six-well plate and incubated at 37 °C for 20 min. The cells were washed three times with a serum-free cell culture medium to completely remove DCFH-DA, which did not enter the cells. A flow cytometer (FACSCalibur, BD Biosciences) was used to detect cellular ROS in the different groups.

4.12. Dual-luciferase reporter assay

The predicted 3′-UTR sequence of *Ccn2* interacting with miR-15b-5p/miR-290a-5p and mutated sequences within the predicted target sites were synthesized and inserted into the pmirGLO control vector (Promega). The insert sequences used for the luciferase reporter assay are listed in Supplementary Table 10. HEK293T cells were transfected with 50 nM miR-15b-5p/miR-290a-5p or negative control and 400 ng of the wild-type or mutant 3′UTR plasmid by Lipofectamine 2000 (Invitrogen). After 48 h of transfection, the luciferase activity of the cells was measured using a Dual Luciferase Assay Kit (Yeasen). Renilla luciferase was used to normalize the value of firefly luciferase.

4.13. Animal experimental procedures

Male C57BL/6 mice (Young mice: 8 weeks; Aged mice: 14 months) were used in this study. There were five young mice (Young), two aged control mice (Ctrl), and five aged mice treated with ESC-EVs (ESC-EV). We randomly divided young mice and ESC-EVs treated aged mice into two groups for cell extraction and sequencing, with two mice in one group and three mice in the other group. Two aged control mice as one group for cell extraction and sequencing. The animal care and experimental procedures were approved by the Animal Research Committee of Nankai University (SYDWLL-000043). Mice were injected with ESC-EVs (100 μg) or an equivalent volume of PBS by intraperitoneal injections once every 2 days for 8 weeks. Mice were sacrificed 24h after the last

injection. Mononuclear cells were isolated from the peripheral blood of mice using Ficoll stratified solution according to the instructions (TBD).

4.14. RNA-sequencing and miRNA-sequencing analysis

Total RNA was isolated and purified using TRIzol reagent (Invitrogen) according to the manufacturer's instructions. The amount and purity of RNA in each sample was quantified using NanoDrop ND-1000. The RNA integrity was assessed using Bioanalyzer 2100 (Agilent) with an RIN number >7.0. Finally, 2×150bp paired-end sequencing (PE150) was performed on an Illumina Novaseq™ 6000 (LC-Bio Technology CO., Ltd.) according to the manufacturer's recommended protocol.

For miRNA-sequencing, approximately 1 μg of total RNA was used to prepare the miRNA library according to the protocol of the TruSeq Small RNA Sample Prep Kits (Illumina). Paired-end sequencing (1×50bp) was then performed on an Illumina Hiseq2500 (LC-Bio Technology CO., Ltd).

4.15. Statistical analysis

Data are expressed as mean ± SEM. Two-tailed Student's t-test was used for comparisons between two groups, and one-way ANOVA was performed for comparisons of data with more than two groups. $P < 0.05$ was considered statistically significant. All experiments were evaluated in at least three independent experiments.

Data availability statement

The data set used and/or analyzed in the current study are available from the corresponding author upon reasonable request. Data for reproducing the rest of the main figures in the paper are provided as supplementary tables.

Declaration of competing interest

The authors declare that there is no conflict of interest regarding the publication of this paper.

Acknowledgements

Appendix A. Supplementary data

Supplementary data to this article can be found online at https://doi.org/10.1016/j.bioactmat.2023.06.011.

References

[1] Y. Hou, X. Dan, M. Babbar, Y. Wei, S.G. Hasselbalch, D.L. Croteau, V.A. Bohr, Ageing as a risk factor for neurodegenerative disease, Nat. Rev. Neurol. 15 (10) (2019) 565–581.

[2] Y. Stern, Cognitive reserve in ageing and Alzheimer's disease, Lancet Neurol. 11 (11) (2012) 1006–1012.

[3] C. Lopez-Otin, M.A. Blasco, L. Partridge, M. Serrano, G. Kroemer, The hallmarks of aging, Cell 153 (6) (2013) 1194–1217.

[4] A. Pouikli, S. Parekh, M. Maleszewska, C. Nikopoulou, M. Baghdadi, I. Tripodi, K. Folz-Donahue, Y. Hinze, A. Mesaros, D. Hoey, P. Giavalisco, R. Dowell, L. Partridge, P. Tessarz, Chromatin remodeling due to degradation of citrate carrier impairs osteogenesis of aged mesenchymal stem cells, Nature Aging 1 (9) (2021) 810–825.

[5] G. Hewitt, D. Jurk, F.D. Marques, C. Correia-Melo, T. Hardy, A. Gackowska, R. Anderson, M. Taschuk, J. Mann, J.F. Passos, Telomeres are favoured targets of a persistent DNA damage response in ageing and stress-induced senescence, Nat. Commun. 3 (2012) 708.

[6] S. Brandhorst, I.Y. Choi, M. Wei, C.W. Cheng, S. Sedrakyan, G. Navarrete, L. Dubeau, L.P. Yap, R. Park, M. Vinciguerra, S. Di Biase, H. Mirzaei, M.G. Mirisola, P. Childress, L. Ji, S. Groshen, F. Penna, P. Odetti, L. Perin, P.S. Conti, Y. Ikeno, B. K. Kennedy, P. Cohen, T.E. Morgan, T.B. Dorff, V.D. Longo, A periodic diet that mimics fasting promotes multi-system regeneration, enhanced cognitive performance, and healthspan, Cell Metabol. 22 (1) (2015) 86–99.

[7] L.M. Redman, S.R. Smith, J.H. Burton, C.K. Martin, D. Il'yasova, E. Ravussin, Metabolic slowing and reduced oxidative damage with sustained caloric restriction support the rate of living and oxidative damage theories of aging, Cell Metabol. 27 (4) (2018) 805–815 e4.

[8] A. Ocampo, P. Reddy, P. Martinez-Redondo, A. Platero-Luengo, F. Hatanaka, T. Hishida, M. Li, D. Lam, M. Kurita, E. Beyret, T. Araoka, E. Vazquez-Ferrer, D. Donoso, J.L. Roman, J. Xu, C. Rodriguez Esteban, G. Nunez, E. Nunez Delicado, J.M. Campistol, I. Guillen, P. Guillen, J.C. Izpisua Belmonte, In vivo amelioration of age-associated hallmarks by partial reprogramming, Cell 167 (7) (2016) 1719–1733, e12.

[9] Z. Chen, W.Y. Chang, A. Etheridge, H. Strickfaden, Z. Jin, G. Palidwor, J.H. Cho, K. Wang, S.Y. Kwon, C. Dore, A. Raymond, A. Hotta, J. Ellis, R.A. Kandel, F. J. Dilworth, T.J. Perkins, M.J. Hendzel, D.J. Galas, W.L. Stanford, Reprogramming progeria fibroblasts re-establishes a normal epigenetic landscape, Aging Cell 16 (4) (2017) 870–887.

[10] L. Lapasset, O. Milhavet, A. Prieur, E. Besnard, A. Babled, N. Ait-Hamou, J. Leschik, F. Pellestor, J.M. Ramirez, J. De Vos, S. Lehmann, J.M. Lemaitre, Rejuvenating senescent and centenarian human cells by reprogramming through the pluripotent state, Genes Dev. 25 (21) (2011) 2248–2253.

[11] S.A. Villeda, K.E. Plambeck, J. Middeldorp, J.M. Castellano, K.I. Mosher, J. Luo, L. K. Smith, G. Bieri, K. Lin, D. Berdnik, R. Wabl, J. Udeochu, E.G. Wheatley, B. Zou, D.A. Simmons, X.S. Xie, F.M. Longo, T. Wyss-Coray, Young blood reverses age-related impairments in cognitive function and synaptic plasticity in mice, Nat. Med. 20 (6) (2014) 659–663.

[12] M. Sinha, Y.C. Jang, J. Oh, D. Khong, E.Y. Wu, R. Manohar, C. Miller, S. G. Regalado, F.S. Loffredo, J.R. Pancoast, M.F. Hirshman, J. Lebowitz, J. L. Shadrach, M. Cerletti, M.J. Kim, T. Serwold, L.J. Goodyear, B. Rosner, R.T. Lee, A.J. Wagers, Restoring systemic GDF11 levels reverses age-related dysfunction in mouse skeletal muscle, Science 344 (6184) (2014) 649–652.

[13] M. Xu, T. Pirtskhalava, J.N. Farr, B.M. Weigand, A.K. Palmer, M.M. Weivoda, C. L. Inman, M.B. Ogrodnik, C.M. Hachfeld, D.G. Fraser, J.L. Onken, K.O. Johnson, G. C. Verzosa, L.G.P. Langhi, M. Weigl, N. Giorgadze, N.K. LeBrasseur, J.D. Miller, D. Jurk, R.J. Singh, D.B. Allison, K. Ejima, G.B. Hubbard, Y. Ikeno, K. Cubro, V. D. Garovic, X. Hou, S.J. Weroha, P.D. Robbins, L.J. Niederhofer, S. Khosla, T. Tchkonia, J.L. Kirkland, Senolytics improve physical function and increase lifespan in old age, Nat. Med. 24 (8) (2018) 1246–1256.

[14] K. Baumann, Rejuvenating senolytics, Nat. Rev. Mol. Cell Biol. 19 (9) (2018) 543.

[15] C. Amor, J. Feucht, J. Leibold, Y.J. Ho, C. Zhu, D. Alonso-Curbelo, J. Mansilla-Soto, J.A. Boyer, X. Li, T. Giavridis, A. Kulick, S. Houlihan, E. Peerschke, S.L. Friedman, V. Ponomarev, A. Piersigilli, M. Sadelain, S.W. Lowe, Senolytic CAR T cells reverse senescence-associated pathologies, Nature 583 (7814) (2020) 127–132.

[16] Y. Cai, H. Zhou, Y. Zhu, Q. Sun, Y. Ji, A. Xue, Y. Wang, W. Chen, X. Yu, L. Wang, H. Chen, C. Li, T. Luo, H. Deng, Elimination of senescent cells by beta-galactosidase-targeted prodrug attenuates inflammation and restores physical function in aged mice, Cell Res. 30 (7) (2020) 574–589.

[17] Y. Zhang, J. Xu, S. Liu, M. Lim, S. Zhao, K. Cui, X. Zhang, L. Wang, Q. Ji, Z. Han, D. Kong, Z. Li, N. Liu, Embryonic stem cell-derived extracellular vesicles enhance the therapeutic effect of mesenchymal stem cells, Theranostics 9 (23) (2019) 6976–6990.

[18] Y. Zhu, J. Ge, C. Huang, H. Liu, H. Jiang, Application of mesenchymal stem cell therapy for aging frailty: from mechanisms to therapeutics, Theranostics 11 (12) (2021) 5675–5685.

[19] S. Golpanian, D.L. DiFede, A. Khan, I.H. Schulman, A.M. Landin, B.A. Tompkins, A. W. Heldman, R. Miki, B.J. Goldstein, M. Mushtaq, S. Levis-Dusseau, J.J. Byrnes, M. Lowery, M. Natsumeda, C. Delgado, R. Saltzman, M. Vidro-Casiano, M.V. Pujol, M. Da Fonseca, A.A. Oliva Jr., G. Green, C. Premer, A. Medina, K. Valasaki, V. Florea, E. Anderson, J. El-Khorazaty, A. Mendizabal, P.J. Goldschmidt-Clermont, J.M. Hare, Allogeneic human mesenchymal stem cell infusions for aging frailty, J Gerontol A Biol Sci Med Sci 72 (11) (2017) 1505–1512.

[20] A.G. Smith, Embryo-derived stem cells: of mice and men, Annu. Rev. Cell Dev. Biol. 17 (2001) 435–462.

[21] M.J. Evans, M.H. Kaufman, Establishment in culture of pluripotential cells from mouse embryos, Nature 292 (5819) (1981) 154–156.

[22] G. Huang, S. Ye, X. Zhou, D. Liu, Q.L. Ying, Molecular basis of embryonic stem cell self-renewal: from signaling pathways to pluripotency network, Cell. Mol. Life Sci. 72 (9) (2015) 1741–1757.

[23] D. Solter, J. Gearhart, Putting stem cells to work, Science 283 (5407) (1999) 1468–1470.

[24] S. Yamanaka, Pluripotent stem cell-based cell therapy-promise and challenges, Cell Stem Cell 27 (4) (2020) 523–531.

[25] O. Caspi, J. Huber, I. Kehat, M. Habib, G. Arbel, A. Gepstein, L. Yankelson, D. Aronson, R. Beyar, L. Gepstein, Transplantation of human embryonic stem cell-derived cardiomyocytes improves myocardial performance in infarcted rat hearts, J. Am. Coll. Cardiol. 50 (19) (2007) 1884–1893.

[26] U. Ben-David, N. Benvenisty, The tumorigenicity of human embryonic and induced pluripotent stem cells, Nat. Rev. Cancer 11 (4) (2011) 268–277.

[27] E. Ford, J. Pearlman, T. Ruan, J. Manion, M. Waller, G.G. Neely, L. Caron, Human pluripotent stem cells-based therapies for neurodegenerative diseases: current status and challenges, Cells 9 (11) (2020).

[28] A.S. Lee, C. Tang, M.S. Rao, I.L. Weissman, J.C. Wu, Tumorigenicity as a clinical hurdle for pluripotent stem cell therapies, Nat. Med. 19 (8) (2013) 998–1004.

[29] E.R. Abels, X.O. Breakefield, Introduction to extracellular vesicles: biogenesis, RNA cargo selection, content, release, and uptake, Cell. Mol. Neurobiol. 36 (3) (2016) 301–312.

[30] G. van Niel, G. D'Angelo, G. Raposo, Shedding light on the cell biology of extracellular vesicles, Nat. Rev. Mol. Cell Biol. 19 (4) (2018) 213–228.

[31] A.F. Saleh, E. Lazaro-Ibanez, M.A. Forsgard, O. Shatnyeva, X. Osteikoetxea, F. Karlsson, N. Heath, M. Ingelsten, J. Rose, J. Harris, M. Mairesse, S.M. Bates, M. Clausen, D. Etal, E. Leonard, M.D. Fellows, N. Dekker, N. Edmunds, Extracellular vesicles induce minimal hepatotoxicity and immunogenicity, Nanoscale 11 (14) (2019) 6990–7001.

[32] M. Adamiak, G. Cheng, S. Bobis-Wozowicz, L. Zhao, S. Kedracka-Krok, A. Samanta, E. Karnas, Y.T. Xuan, B. Skupien-Rabian, X. Chen, U. Jankowska, M. Girgis, M. Sekula, A. Davani, S. Lasota, R.J. Vincent, M. Sarna, K.L. Newell, O.L. Wang, N. Dudley, Z. Madeja, B. Dawn, E.K. Zuba-Surma, Induced pluripotent stem cell (iPSC)-Derived extracellular vesicles are safer and more effective for cardiac repair than iPSCs, Circ. Res. 122 (2) (2018) 296–309.

[33] J.A. Fafian-Labora, A. O'Loghlen, Classical and nonclassical intercellular communication in senescence and ageing, Trends Cell Biol. 30 (8) (2020) 628–639.

[34] B. Chen, Y. Sun, J. Zhang, Q. Zhu, Y. Yang, X. Niu, Z. Deng, Q. Li, Y. Wang, Human embryonic stem cell-derived exosomes promote pressure ulcer healing in aged mice by rejuvenating senescent endothelial cells, Stem Cell Res. Ther. 10 (1) (2019) 142.

[35] Y.U. Bae, Y. Son, C.H. Kim, K.S. Kim, S.H. Hyun, H.G. Woo, B.A. Jee, J.H. Choi, H. K. Sung, H.C. Choi, S.Y. Park, J.H. Bae, K.O. Doh, J.R. Kim, Embryonic stem cell-derived mmu-miR-291a-3p inhibits cellular senescence in human dermal fibroblasts through the TGF-beta receptor 2 pathway, J Gerontol A Biol Sci Med Sci 74 (9) (2019) 1359–1367.

[36] L. Gong, B. Chen, J. Zhang, Y. Sun, J. Yuan, X. Niu, G. Hu, Y. Chen, Z. Xie, Z. Deng, Q. Li, Y. Wang, Human ESC-sEVs alleviate age-related bone loss by rejuvenating senescent bone marrow-derived mesenchymal stem cells, J. Extracell. Vesicles 9 (1) (2020), 1800971.

[37] G. Hu, Y. Xia, B. Chen, J. Zhang, L. Gong, Y. Chen, Q. Li, Y. Wang, Z. Deng, ESC-sEVs rejuvenate aging hippocampal NSCs by transferring SMADs to regulate the MYT1-egln3-sirt1 Axis, Mol. Ther. 29 (1) (2021) 103–120.

[38] W.S. Toh, R.C. Lai, B. Zhang, S.K. Lim, MSC exosome works through a protein-based mechanism of action, Biochem. Soc. Trans. 46 (4) (2018) 843–853.

[39] G. Qiu, G. Zheng, M. Ge, J. Wang, R. Huang, Q. Shu, J. Xu, Mesenchymal stem cell-derived extracellular vesicles affect disease outcomes via transfer of microRNAs, Stem Cell Res. Ther. 9 (1) (2018) 320.

[40] D.P. Bartel, MicroRNAs: genomics, biogenesis, mechanism, and function, Cell 116 (2) (2004) 281–297.

[41] T. Su, Y. Xiao, Y. Xiao, Q. Guo, C. Li, Y. Huang, Q. Deng, J. Wen, F. Zhou, X.H. Luo, Bone marrow mesenchymal stem cells-derived exosomal MiR-29b-3p regulates aging-associated insulin resistance, ACS Nano 13 (2) (2019) 2450–2462.

[42] Y. Zhang, M.S. Kim, B. Jia, J. Yan, J.P. Zuniga-Hertz, C. Han, D. Cai, Hypothalamic stem cells control ageing speed partly through exosomal miRNAs, Nature 548 (7665) (2017) 52–57.

[43] Y. Zeng, C. Du, P. Xiao, Y. Lei, P. Zhao, Z. Zhu, S. Gao, B. Chen, S. Cheng, W. Huang, C. Zhao, Sox9-Increased miR-322-5p facilitates BMP2-induced chondrogenic differentiation by targeting Smad7 in mesenchymal stem cells, Stem Cell. Int. 2021 (2021), 9778207.

[44] S. Yu, Y. Lu, A. Su, J. Chen, J. Li, B. Zhou, X. Liu, Q. Xia, Y. Li, J. Li, M. Huang, Y. Ye, Q. Zhao, S. Jiang, X. Yan, X. Wang, C. Di, J. Pan, S. Su, A CD10-OGP membrane peptolytic signaling Axis in fibroblasts regulates lipid metabolism of cancer stem cells via SCD1, Adv. Sci. 8 (19) (2021), e2101848.

[45] N. Suh, MicroRNA controls of cellular senescence, BMB Rep 51 (10) (2018) 493–499.

[46] L.J. Mah, A. El-Osta, T.C. Karagiannis, GammaH2AX as a molecular marker of aging and disease, Epigenetics 5 (2) (2010) 129–136.

[47] Z. Jing, X. Yuan, J. Zhang, X. Huang, Z. Zhang, J. Liu, M. Zhang, J. Oyang, Y. Zhang, Z. Zhang, R. Yang, Chromosome 1 open reading frame 190 promotes activation of NF-kappaB canonical pathway and resistance of dendritic cells to tumor-associated inhibition in vitro, J. Immunol. 185 (11) (2010) 6719–6727.

[48] J.I. Jun, L.F. Lau, CCN2 induces cellular senescence in fibroblasts, J Cell Commun Signal 11 (1) (2017) 15–23.

[49] J.I. Jun, L.F. Lau, The matricellular protein CCN1 induces fibroblast senescence and restricts fibrosis in cutaneous wound healing, Nat. Cell Biol. 12 (7) (2010) 676–685.

[50] K.H. Kim, C.C. Chen, R.I. Monzon, L.F. Lau, Matricellular protein CCN1 promotes regression of liver fibrosis through induction of cellular senescence in hepatic myofibroblasts, Mol. Cell Biol. 33 (10) (2013) 2078–2090.

[51] I.T. Moe, T.A. Pham, E.M. Hagelin, M.S. Ahmed, H. Attramadal, CCN2 exerts direct cytoprotective actions in adult cardiac myocytes by activation of the PI3-kinase/Akt/GSK-3beta signaling pathway, J Cell Commun Signal 7 (1) (2013) 31–47.

[52] Z. Wu, C. Zhou, Q. Yuan, D. Zhang, J. Xie, S. Zou, CTGF facilitates cell-cell communication in chondrocytes via PI3K/Akt signalling pathway, Cell Prolif. 54 (3) (2021), e13001.

[53] M. Scudellari, Ageing research: blood to blood, Nature 517 (7535) (2015) 426–429.

[54] A. Sahu, Z.J. Clemens, S.N. Shinde, S. Sivakumar, A. Pius, A. Bhatia, S. Picciolini, C. Carlomagno, A. Gualerzi, M. Bedoni, B. Van Houten, M. Lovalekar, N.F. Fitz, I. Lefterov, A. Barchowsky, R. Koldamova, F. Ambrosio, Regulation of aged skeletal muscle regeneration by circulating extracellular vesicles, Nature Aging 1 (12) (2021) 1148–1161.

[55] S. Ancel, J.N. Feige, Young extracellular vesicles rejuvenate aged muscle, Nature Aging 1 (12) (2021) 1078–1080.

[56] Y.U. Bae, J.H. Choi, A. Nagy, H.K. Sung, J.R. Kim, Antisenescence effect of mouse embryonic stem cell conditioned medium through a PDGF/FGF pathway, Faseb. J. 30 (3) (2016) 1276–1286.

[57] J. Sanz-Ros, N. Romero-Garcia, C. Mas-Bargues, D. Monleon, J. Gordevicius, R. T. Brooke, M. Dromant, A. Diaz, A. Derevyanko, A. Guio-Carrion, A. Roman-Dominguez, M. Ingles, M.A. Blasco, S. Horvath, J. Vina, C. Borras, Small extracellular vesicles from young adipose-derived stem cells prevent frailty, improve health span, and decrease epigenetic age in old mice, Sci. Adv. 8 (42) (2022) eabq2226.

[58] W. Hu, C.S. Chan, R. Wu, C. Zhang, Y. Sun, J.S. Song, L.H. Tang, A.J. Levine, Z. Feng, Negative regulation of tumor suppressor p53 by microRNA miR-504, Mol. Cell 38 (5) (2010) 689–699.

[59] M. Kumar, Z. Lu, A.A. Takwi, W. Chen, N.S. Callander, K.S. Ramos, K.H. Young, Y. Li, Negative regulation of the tumor suppressor p53 gene by microRNAs, Oncogene 30 (7) (2011) 843–853.

[60] J.I. Jun, L.F. Lau, Taking aim at the extracellular matrix: CCN proteins as emerging therapeutic targets, Nat. Rev. Drug Discov. 10 (12) (2011) 945–963.

[61] C.C. Chen, L.F. Lau, Functions and mechanisms of action of CCN matricellular proteins, Int. J. Biochem. Cell Biol. 41 (4) (2009) 771–783.

[62] K.P. Holbourn, K.R. Acharya, B. Perbal, The CCN family of proteins: structure-function relationships, Trends Biochem. Sci. 33 (10) (2008) 461–473.

[63] F. Momen-Heravi, Isolation of extracellular vesicles by ultracentrifugation, Methods Mol. Biol. 1660 (2017) 25–32.

[64] L. Yu, S. Liu, C. Wang, C. Zhang, Y. Wen, K. Zhang, S. Chen, H. Huang, Y. Liu, L. Wu, Z. Han, X. Chen, Z. Li, N. Liu, Embryonic stem cell-derived extracellular vesicles promote the recovery of kidney injury, Stem Cell Res. Ther. 12 (1) (2021) 379.